Biosensors and Bioelectronics xx (xxxx) xxxx–xxxx

Contents lists available at ScienceDirect

Biosensors and Bioelectronics

journal homepage: www.elsevier.com/locate/bios

A new sight for detecting the ADRB1 gene mutation to guide a therapeutic regimen for hypertension based on a CeO_2-doped nanoprobe

Yilin Zhao[1], Junlin He[1], Yazhen Niu, Jun Chen, Jing Wu, Chao Yu*

Institute of Life Science, College of Pharmacy and School of Public Health, Chongqing Medical University, Chongqing 400016, PR China

ARTICLE INFO

Keywords:
CeO_2
Biotin-avidin system
The β1-adrenergic receptor gene
Target therapy

ABSTRACT

The β1-adrenergic receptor gene (Entrez Gene:*ADRB1*), as the target of beta-blockers for hypertension, can directly influence the antihypertensive effect of metoprolol in the Chinese population. This therapeutic effect is often hindered by a lack of evidence-based medical information. To address this challenge, we report a novel assay based on graphene oxide and a CeO_2 nanocomposite functionalized by 3-aminopropyltriethoxysilane supported Pt nanoparticles (GO/CeO_2/PtNPs) as a signal probe. Due to the large specific surface area and good adsorption properties of the GO/CeO_2 nanocomposite, large amounts of PtNPs were immobilized, which amplified the electrochemical signal and improved the sensitivity of the biosensor. To further improvement the sensitivity of the biosensor, Streptavidin (SA) was introduced because it can provide more active sites for the immobilization of the biotinylated capture probe (bio-CP). The electrochemical signal was primarily derived from the catalysis of H_2O_2 by GO/CeO_2/PtNPs. Chronoamperometry was applied to record electrochemical signals, which linearly increased with target DNA. Under optimal conditions, the prepared biosensor had a wide linear range from 1 fM to 10 nM and a low detection limit of 0.33 fM in the detecting of ADRB1 gene. Moreover, the proposed method had good stability and recovery, suggesting its potential for use in clinical research.

1. Introduction

The β1-adrenergic receptor gene (Entrez Gene:*ADRB1*) is known to be the target of beta-blockers for hypertension (Thomas et al., 2010). The ADRB1 gene has a common single nucleotide polymorphism (SNP), ADRB1 Arg389Gly (rs1801253,c.1165G > C), which can directly influence the antihypertensive effect of metoprolol in the Chinese population with hypertension (Jiang et al., 2011). Hypertensive patients with Gly389Arg, which is caused by the 1165G > C SNP, need larger doses than who carrying heterozygous Arg389Arg (Jiang et al., 2011). Therefore, it is crucial to prescreen patients to determine their genotypes before using this drug to minimize the risk of the adverse reactions and provide guidance for clinical personalized therapy.

Various techniques for ADRB1 genotyping via prescreening have been reported, such as DNA sequencing (Kang et al., 2015) and real-time quantitative polymerase chain reaction (qPCR) (Lima et al., 2007; Nicoulina et al., 2010). DNA sequencing requires a great deal of preliminary work (Carson and Wanunu, 2015), and qPCR is poorly suited for implementation due to the complicated sample pre-treatment, high cost, relatively long detection time, and likelihood of false or negative results (Jiang et al., 2011). Compared with the above methods, DNA biosensors have received a large amount of attention because of their simplicity, rapidity, low cost, minimal sample preparation, and short response time (Li et al., 2016). Thus, finding a highly sensitive and selective DNA-based electrochemical sensor for ADRB1 mutation detection appears to be a realistic goal.

Cerium oxide (CeO_2) is an interesting metal oxide due to its unique catalysis properties and the high mobility of oxygen vacancies at the surface, leading to extensive applications in the field of catalysis in the form of pure CeO_2 or doped/loaded with transition metal components (Zhang et al., 2012). Although it has certain catalysis properties toward H_2O_2, the stability of CeO_2 needs to be improved to further amplify the signal and improve the sensitivity of the biosensor. For this purpose, graphene oxide (GO) was used here due to its high surface area-to-volume ratio, good electron transfer properties, high mechanical strength and good water dispersibility (Wei et al., 2016). To use catalysis in the form of CeO_2 loaded with transition metal components, platinum nanoparticles (PtNPs) were chosen owing to its high aspect ratio, evident catalysis, and strong adsorption to thiol and amino groups (Zhang et al., 2014). Meanwhile, PtNPs not only improve the ability of the biosensor but are also used to immobilize the capture probe. In general, the combination of GO and CeO_2 enhanced the

* Correspondence to: College of Pharmacy, Chongqing Medical University, No.1, Box 380#, Yi Xue Yuan Road, Chongqing, Yuzhong district 400016, PR China.
E-mail address: yuchaom@163.com (C. Yu).
[1] Authors contributed equally to this work.

http://dx.doi.org/10.1016/j.bios.2016.10.087
Received 26 August 2016; Received in revised form 12 October 2016; Accepted 28 October 2016
Available online xxxx
0956-5663/

loading capacity of PtNPs and the stability of the biosensor. Furthermore, the PtNPs improved catalysis in the construction of the biosensor (Wei et al., 2016).

Herein, an ultrasensitive DNA biosensor based on biotinylated DNA was used as a capture probe (bio-CP) and GO/CeO_2/PtNPs composites were used as syncatalytic amplifiers to enable the detection of the ADRB1 gene mutation. First, for immobilization of bio-CP, Streptavidin (SA) was introduced during biosensor fabrication because it can provide more active sites for the immobilization of bio-CP. Furthermore, gold nanoparticles (AuNPs) were employed to immobilize SA. The sensitivity of the method was significantly increased with the syncatalytic effect of CeO_2 and PtNPs in the GO/CeO_2/PtNPs nanocomposite. GO/CeO_2/PtNPs and biotin-streptavidin system in our system have the following two major advantages: (1) compared with individual CeO_2 and PtNPs, our synthesized GO/CeO_2/PtNPs have a more efficient catalytic ability because of the syncatalysis of H_2O_2 by CeO_2 and PtNPs, and (2) the biotin-streptavidin system not only provides an active site for the immobilization of bio-CP but also improves the sensitivity of the proposed electrochemical DNA sensor. In order to prove the use of SA is necessary for the construction of the biosensor, the comparison between the biosensor which use SA and that without SA was shown in Scheme 1B. The strategy reported here paves the way for the determination of gene-related mutated nucleotides in biosamples.

2. Experimental

2.1. Materials and chemicals

Graphene Oxide (GO) was provided by Nanjing XFNANO Materials TECH Co., Ltd. (China). Gold (III) chloride trihydrate ($HAuCl_4{\cdot}4H_2O$), Chloroplatinic acid (H_2PtCl_6), streptavidin (SA), cerium (III) nitrate hexahydrate ($Ce(NO_3)_3{\cdot}6H_2O$) and hexamethylenetetramine (HMTA) were obtained from Sigma-Aldrich (St. Louis, USA, www.sigmaaldrich.com). Bovine Serum Albumin (BSA), potassium ferricyanide ($K_3Fe(CN)_6$) and potassium ferrocyanide ($K_4Fe(CN)_6$) were purchased from the Beijing Chemical Reagents Company (Beijing, China). Clinical serum samples were obtained from the First Affiliated Hospital of Chongqing medical university (Chongqing, China). The DNA oligonucleotides, which are illustrated in Table S1, were synthesized and purified by Sangon Biotechology, Inc. (Shanghai, China).

The buffer solutions involved in this study were as follow: 1×TE buffer (10 mM Trishydroxymethylaminomethane hydrochloride (Tris-HCl), and 1.0 mM ethylenediaminetetraacetic acid (EDTA), pH 8.0), which was used to dissolve all oligonucleotides. The other buffer solutions are listed in Table S2. All other reagents were of analytical reagent grade and used without further purification. Ultrapure water (> 18.2 MΩ) obtained from a Millipore Mill-Q purification system was used throughout the experiment.

2.2. Apparatus and characterization

All electrochemical experiments were carried out on a CHI660E electrochemical workstation (Chenhua Instruments Co., Shanghai, China). Scanning electron microscopy (SEM) images were obtained using a Hitachi S-3000N (Hitachi Limited, Japan). Field emission scanning electron microscopy (FE-SEM) image was conducted using a Hitachi S4800 (Hitachi Limited, Japan). Fourier transform-infrared (FT-IR) spectra were collected using a Nicolet 6700 FT-IR spectrometer with KBr pressed disks (Thermo Nicolet, USA). Energy dispersive X-ray spectroscopy (EDS) was measured using a JEOL JSM-6700F microscope (Japan). A conventional three-electrode system was used for all electrochemical measurements: a platinum wire electrode as the counter electrode, a saturated calomel electrode (SCE) as the reference electrode, and a modified glassy carbon electrode (GCE, 4 mm in diameter) as the working electrode.

2.3. Preparation of GO/CeO_2

GO/CeO_2 composites were synthesized by the method described previously with slight modification (Ujjain et al., 2014). First, 10 mg of GO was dissolved in 5 mL of ultrapure water under ultrasonication for 0.5 h to form a homogenous colloidal suspension of exfoliated GO. Next, 10 mL of 0.025 M $Ce(NO_3)_3{\cdot}6H_2O$ was mixed with 10 mL of 0.025 M of HTMA. Then, both solutions were mixed and kept in a water bath at 80 °C for 5 h and filtered followed by repeated washing with ultrapure water. Finally, the obtained precipitate was dried at 60 °C under reduced pressure.

Subsequently, 20 mg of GO-CeO_2 composites was dispersed in 5 mL of ethanol and ultrasonicated for 15 min to obtain symmetrical dispersions. Then, 0.1 mL of APTES was added and kept in reflux at 70 °C for 1.5 h. After cooling to room temperature, the obtained GO/CeO_2 composites were isolated by centrifugation at 8000 rpm for 5 min and washed three times with ultrapure water. Finally, the prepared products were dried at 50 °C for 12 h before further use.

2.4. Preparation of GO/CeO_2/PtNPs

GO/CeO_2/PtNPs nanocomposites were synthesized using the $NaBH_4$ reduction method. Briefly, 1 mL of H_2PtCl_6 (1%) was added to 1 mL of a (2 mg mL^{-1}) GO-CeO_2 solution and vigorously sonicated for 10 min. Then, 2 mL of a $NaBH_4$ (0.1 M) solution was dropwise added into the mixture with stirring for 30 min, followed by centrifugation and washing with ultrapure water and dissolution in 1 mL of ultrapure water for further use.

2.5. Synthesis of PtNPs, GO/PtNPs and GO/CeO_2/AuNPs

GO/CeO_2/AuNPs were synthesized by the $NaBH_4$ reduction method. Briefly, 1 mL of $HAuCl_4{\cdot}4H_2O$ (1%) was added into 1 mL of a (2 mg mL^{-1}) GO/CeO_2 solution and sonicated for 10 min. Then, 2 mL of a $NaBH_4$ (0.1 M) solution was slowly added into the above mixture with stirring for 30 min, followed by centrifugation and washing with ultrapure water. GO/PtNPs composites were synthesized with a similar method for GO/CeO_2/AuNPs preparation, except that 1 mL of (2 mg mL^{-1}) GO/CeO_2 was displaced by 1 mL of (2 mg mL^{-1}) GO. PtNPs were also synthesized as follows. First, 1 mL of H_2PtCl_6 (1%) was added into 1 mL of ultrapure water. Then, 2 mL of a $NaBH_4$ (0.1 M) solution was slowly added into the above mixture with stirring for 30 min, followed by centrifugation and washing with ultrapure water.

2.6. Preparation of GO/CeO_2/PtNPs/SP, GO/CeO_2/AuNPs/SP, GO/PtNPs/SP and PtNPs/SP

In brief, 200 μL of a 1 μm thiol-modified signal probe (SP) was mixed with 1 mL of as-prepared GO/CeO_2/PtNPs and stirred gently overnight at 4 °C. Afterward, 1 mg of BSA that was suspended in 1 mL of TE buffer was added, and the mixture was allowed to further react for another 4 h at 4 °C for blocking the nonspecific binding sites on the surface of the GO/CeO_2/PtNPs. The product was obtained by centrifuging, washing, and recentrifuging, followed by dispersal in 1 mL of hybridization buffer for further use. The preparation process of GO/CeO_2/PtNPs/SP is shown in Scheme 1A. The GO/CeO_2/AuNPs/SP bioconjugates were synthesized with a similar process for GO/CeO_2/PtNPs/SP, except that GO/CeO_2/PtNPs were displaced by GO/CeO_2/AuNPs. Furthermore, GO/PtNPs/SP and PtNPs/SP bioconjugates were also synthesized with an analogous process for GO/CeO_2/PtNPs/SP, except that GO/CeO_2/PtNPs were displaced by GO/PtNPs and PtNPs, respectively.

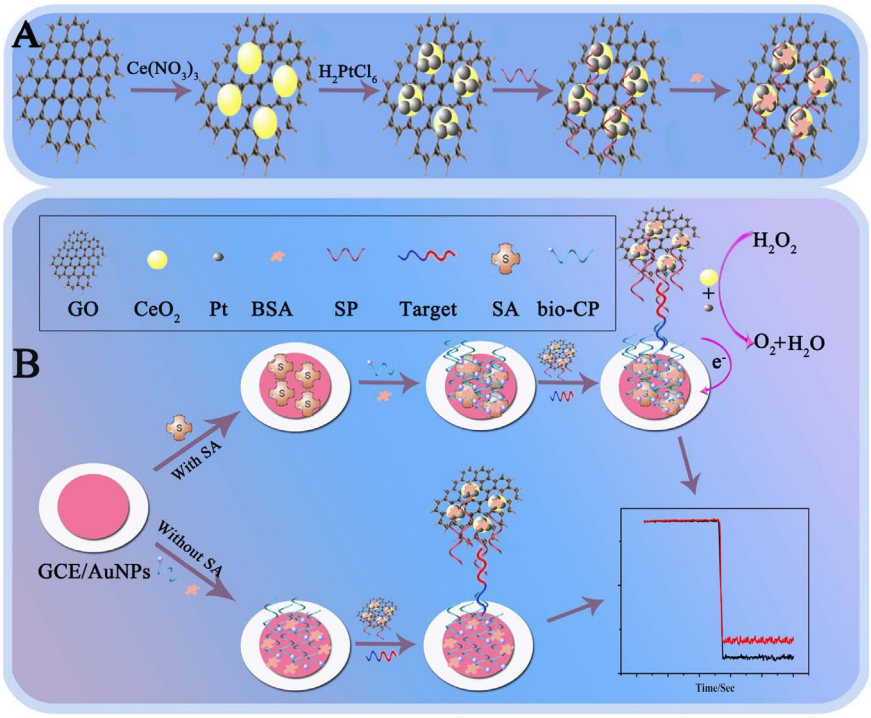

Scheme 1. (A) The preparation process of the signal probes as GO/CeO_2/PtNPs/SP. (B) Schematic representation of the proposed strategy for the DNA biosensor.

2.7. Fabrication of the sensing interfaces

Scheme 1B shows the preparation procedure of the biosensor. Prior to modification, GCE was polished with alumina slurries of 0.3 and 0.05 μm, and the electrode was then sequentially sonicated in water, ethanol and water for 5 min. After being dried at room temperature, the electrode was modified with AuNPs using electrodeposition in a 1.0 wt% $HAuCl_4$ solution at −0.2 V for 30 s. After washing with ultrapure water, 10 μL of a SA solution (100 μg mL^{-1}) was dropped onto the prepared GCE for 12 h at 4 °C via the Au-NH_2 bonding to immobilize SA. After the reaction, the electrodes were washed with ultrapure water to remove loosely bound SA and dried in air. Then, 10 μL of 1 μm bio-CP was dropped onto the GCE/AuNPs and incubated at room temperature for 12 h. After that, the modified electrode was rinsed with ultrapure water and blocked with 10 μL of 1% BSA for 30 min at 37 °C to prevent nonspecific adsorption. The as-prepared DNA biosensor (GCE/AuNPs/SA/bio-CP/BSA) was hybridized with various concentrations of target DNA for 2 h at 37 °C.

2.8. Electrochemical measurements

Detection was based on the typical procedures of the sandwich reaction (Dong et al., 2012; Li et al., 2015). The obtained GCE/AuNPs/SA/bio-CP/BSA/target was immersed in the prepared GO/CeO_2/PtNPs/SP solution for 2 h at 37 °C, followed by washing with washing buffer to remove nonspecific adsorption of the conjugate. Ultimately, electrochemical detection of amperometric i–t curves was recorded at 0.4 V in 7 mL of PBS at room temperature. When the background current was stable, 20 μL of H_2O_2 (1.4 mol L^{-1}) was added to the solution, and the current changes were recorded.

3. Results and discussion

3.1. Characteristics of the modified electrodes

The DNA biosensor fabrication processes were investigated by SEM. After the electrodeposition step, AuNPs were uniformly distributed on the surface of the GCE, and the average size of the AuNPs was approximately 300 nm, as shown in Fig. S1A. Upon immobilization of SA via Au-NH_2 covalent bonds, proteins were trapped on the surface of the AuNPs and a blurry surface image was observed, distinct from that shown in Fig. S1A. This result is indicative of successful SA bonding on the surface of AuNPs. Afterwards, with the immobilization of bio-CP onto the AuNPs/SA film in Fig.S1 C, the size of the AuNPs increased distinctly compared to that shown in Fig. S1B, indicating that bio-CP was successfully introduced via specific recognition between SA and biotin (Zhu et al., 2015).

A comparison of different electrodeposition times of AuNPs was investigated by SEM to confirm the best conditions for the remaining experiment. From Fig. 1A–F, the electrodepositon times were 5 s, 10 s, 15 s, 20 s, 30 s, and 40 s, respectively. The background of the electrode surface in Fig. 1B was filled with AuNPs compared with Fig. 1A, and the average size of AuNPs was approximately 200 nm. With the extension of the electrodeposition time in Fig. 1C-E, the background of the electrode surface reached saturation at 30 s and the average size of AuNPs was enlarged to approximately 300 nm. In contrast, after a further extension of electrodeposition time to 40 s, the background of the electrode surface has no significant difference from that in Fig. 1E, but the size of AuNPs became irregular owing to the fact that the further extension of electrodeposition time caused AuNP stacking, which might influence the electroperformance of the electrode (Gao et al., 2014). As a result, 30 s was chosen for the electrodepositon time of $HAuCl_4$.

3.2. Characterization of the detection probes

To demonstrate successful formation of the detection probes, SEM, FE-SEM, FT-IR spectroscopy and EDS were used. As shown in Fig. 2A, the GO sheets showed a typical flake-like shape with slight wrinkles, similar to the observations of a previous report (Yang et al., 2014). Fig. 2B shows the typical structure of CeO_2, which is in accordance with previously reported results (Ujjain et al., 2014). After reacting with $Ce(NO_3)_3{\cdot}6H_2O$, as shown in Fig. 2C, the as-obtained CeO_2 were well dispersed on GO with an average diameter of approximately 300 nm.

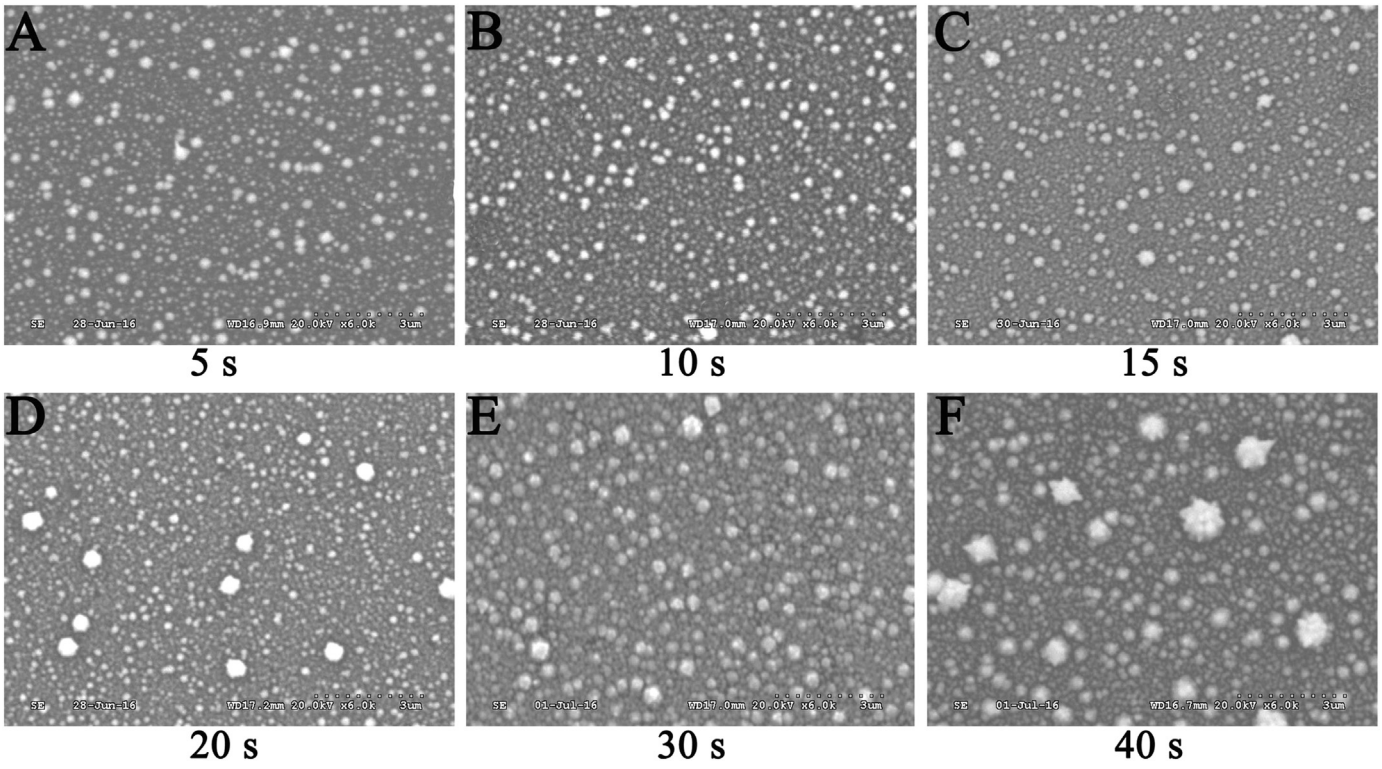

Fig. 1. The morphology change in regard to different electrodepositon times on the electrode surface. (A) 5 s, (B) 10 s, (C) 15 s, (D) 20 s, (E) 30 s and (F) 40 s.

In addition, SEM of GO/CeO_2/PtNPs confirmed that the PtNPs were distributed on the surface of CeO_2 (Fig. 2D). FT-IR was used to further confirm the successful formation of GO/CeO_2. As shown in Fig. 2E, CeO_2 (curve a) shows an absorption band at 1350 and 1530 cm^{-1}. The absorption peak at 1350 cm^{-1} is indicative of the N=O stretching vibration from traces of nitrate (Tang et al., 2013). The absorption peak at 1530 cm^{-1} was observed corresponding to the O–H stretching and the bending vibrations of water adsorbed from the moisture in the air (Tang et al., 2013). The FT-IR spectrum of GO (curve b) showed several obvious peaks at 1750, 1620, 1400 and 1050 cm^{-1}, representing the stretching vibrations of C=O, C=C, O–H and C–O, respectively (Gao et al., 2014). Compared with curve a and b, curve c shows absorption bands at 1200, 2850 and 2930 cm^{-1}. Owing to the conjugated effect between GO and CeO_2, the absorption peek of CeO_2 at 1350 cm^{-1} was

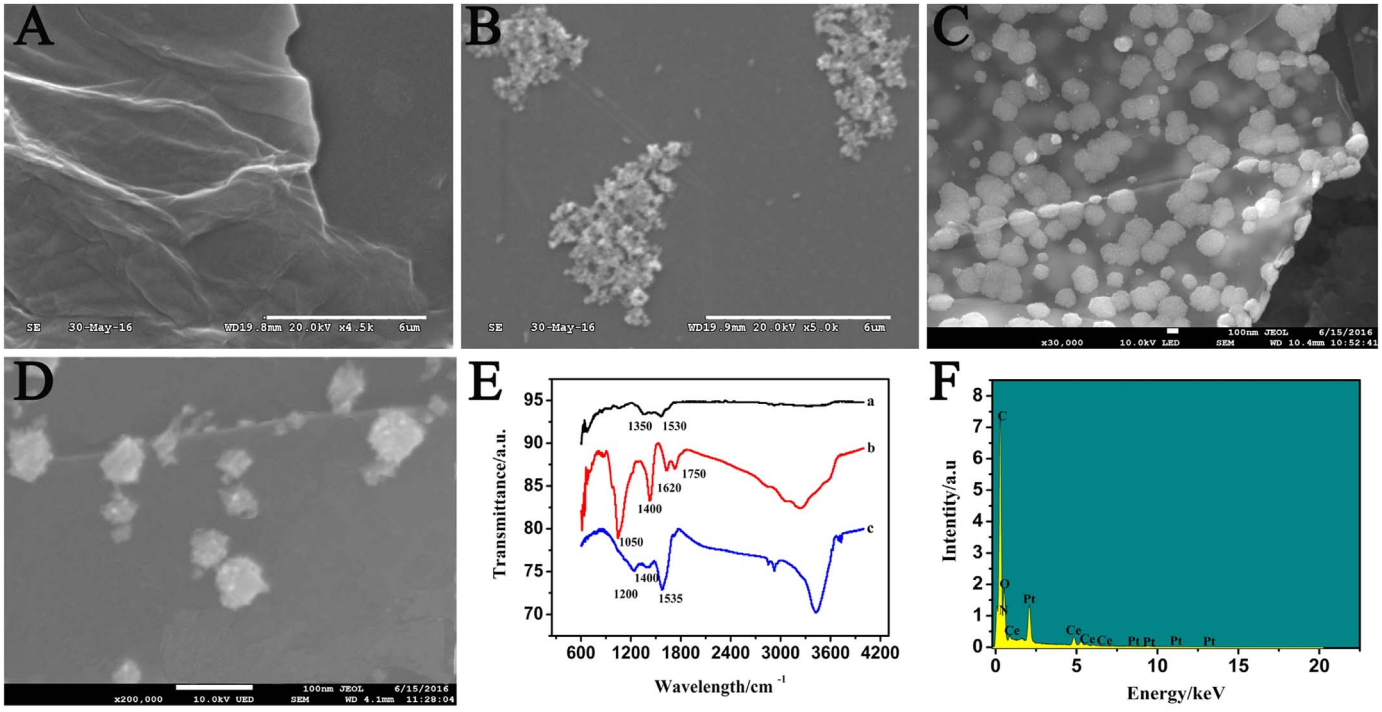

Fig. 2. SEM images of (A) GO and (B) CeO_2; FE-SEM of (C) GO/CeO_2 and (D) GO/CeO_2/PtNPs; (E) FT-IR spectra of (a) CeO_2, (b) GO and (c) GO/CeO_2; and EDS of (F) GO/CeO_2/PtNPs hybrids. (For interpretation of the references to color in this figure legend, the reader is referred to the web version of this article).

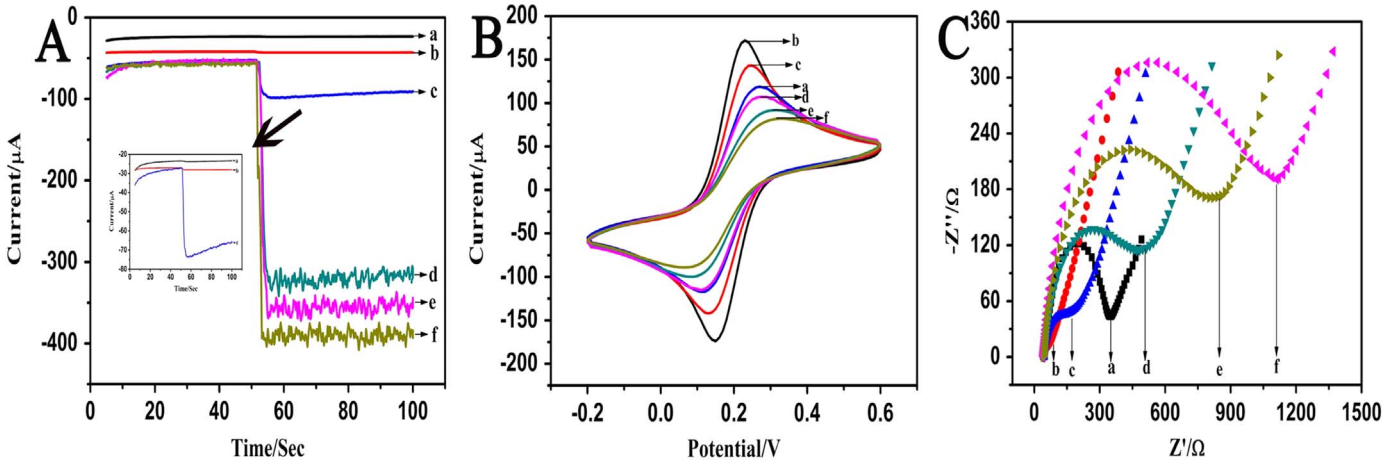

Fig. 3. (A) The Amperometric i-t curves of different nanomaterial: (a) GO, (b) CeO_2, (c) GO- CeO_2, (d) Pt, (e) GO/PtNPs and (f) GO/CeO_2/PtNPs; (B) CV characterization of electrodes at various stages of modification in a 5 mM $[Fe(CN)_6]^{3-/4-}$ solution: (a) bare GCE, (b) GCE/AuNPs, (c) GCE/AuNPs/SA, (d) GCE/AuNPs/SA/bio-CP, (e) GCE/AuNPs/SA/bio-CP/BSA and (f) GCE/AuNPs/SA/bio-CP/BSA/target DNA; (B) EIS for each immobilization step in 5 mM $[Fe(CN)_6]^{3-/4-}$: (a) bare GCE, (b) GCE/AuNPs, (c) GCE/AuNPs/SA, (d) GCE/AuNPs/SA/bio-CP, (e) GCE/AuNPs/SA/bio-CP/BSA and (f) GCE/AuNPs/SA/bio-CP/BSA/target DNA.

red shifted to 1200 cm^{-1}. To further monitor the formation of GO/CeO_2/PtNPs, EDS characterization was employed. As shown in Fig. 2F, several intense peaks of Pt were observed, suggesting that PtNPs were successfully modified on GO/CeO_2. From these results, it could be observed that the GO/CeO_2/PtNPs had been successfully synthesized.

Successful coupling among the target DNA, bio-CP and SP was investigated by agarose gel electrophoresis. In Fig. S2, bio-CP (lane a) showed the highest mobility due to its low molecular weight, as expected, and bio-CP-target DNA conjugates (lane c) showed lower mobility than target DNA (lane b) and bio-CP. The above results confirmed the successful hybridization of bio-CP and target DNA. Further, compared with SP (lane d), lane e had the same volume of bio-CP and SP added and had no significant mobility change, but the band intensity was weakened because bio-CP cannot hybridize with SP. To confirm the successful hybridization of SP and target DNA, lane f shows the results that SP can hybridize with the target and have a lower mobility than lane d. Finally, lane g shows the lowest mobility, which confirmed that target DNA can hybridize with bio-CP and SP. These results demonstrated the hybridization feasibility of our DNA biosensor.

3.3. The electrochemical behaviour of different nanomaterials for signal tags

Amperometric i-t curves were used to confirm the successful synthesis of GO-CeO_2-PtNPs and to compare the electrochemical behaviours of different nanomaterials. As shown in Fig. 3A, curve a shows the i-t responses of GO, which identified GO as having no catalytic ability with H_2O_2. Compared with GO, CeO_2 (curve b) shows some catalytic ability, which can be seen in the inset and partially enlarged details of curves a, b and c. This result confirmed that CeO_2 can catalyse H_2O_2 (Ujjain et al., 2014). After CeO_2 was grown on GO, the synthesis of GO/CeO_2 (curve c) showed an enhanced catalysis curve compared with curve a and b, owing to the large surface of GO, which can load more CeO_2 and further enhance the catalytic ability. Finally, when PtNPs were reduced on the surface of CeO_2, the catalytic ability was obviously increased (curve f) due to the syncatalytic effect of CeO_2 and PtNPs. Moreover, curves d and e show the electrochemical response of PtNPs and GO/PtNPs. The results demonstrate that the nanomaterial used in this biosensor has the best catalytic ability among the other materials in this experiment.

3.4. Electrochemical behaviour of the DNA biosensor

As shown in Fig. 3B, CV experiments were performed to monitor the stepwise modification procedure of the electrodes in a 5 mM $[Fe(CN)_6]^{3-/4-}$ solution. Compared with bare GCE (curve a), the peak current increased dramatically after AuNPs were electrodeposited on bare GCE (curve b), which was ascribed to the fact that AuNPs have good conductivity and can amplify the electrochemical signal. When the modified electrode was incubated with SA (curve c), the peak current decreased due to the poor conductivity of SA. After bio-CP was assembled onto the electrode surface, the peak current obviously decreased (curve d), which accounts for the fact that bio-CP can hinder the diffusion of ferricyanide toward the electrode surface. BSA as a blocking agent made the peak current decrease again (curve e). Additionally, the peak current further decreased after incubation with the target DNA (ADRB1), which was attributed to the fact that negatively charged DNA was loaded on the electrode surface, inhibiting the diffusion of the redox probe.

In addition, the fabrication processes of the biosensor were also confirmed by electrochemical impedance spectroscopy (EIS) at 5 mM $[Fe(CN)_6]^{3-/4-}$. The impedance spectra included a linear portion and a semicircle portion. The semicircle diameter is equal to the electron transfer resistance, and the linear part of the curve at low frequency represents the diffusion process. As shown in Fig. 3C, curve a shows that the bare GCE exhibited a small semicircle at high frequency. Compared with curve a, after the electro-deposition of AuNPs, the resistance decreased (curve b), indicating that AuNPs promoted electron transfer between the electrode and solution. Then, a large semicircle diameter was observed when SA was dropped onto the electrode (curve c), implying that SA was successively immobilized onto the electrode and blocked electron transfer. After the electrode was incubated with bio-CP (curve e), the resistance increased dramatically because negatively charged DNA electrostatically repels negatively charged redox species. A larger semicircle diameter of curve f was later found, confirming that the prepared biosensor was blocked with BSA. Subsequently, the resistance of curve g increased again, indicating the successful capture of target DNA (ADRB1) and the formation of a complex layer, blocking electron transfer.

3.5. Comparison of different signal-amplification Strategies

To test the signal amplification of the proposed protocol, the biosensor was utilized with different signal amplification strategies with the same concentration (100 fM) of target DNA (Fig. 4). Three

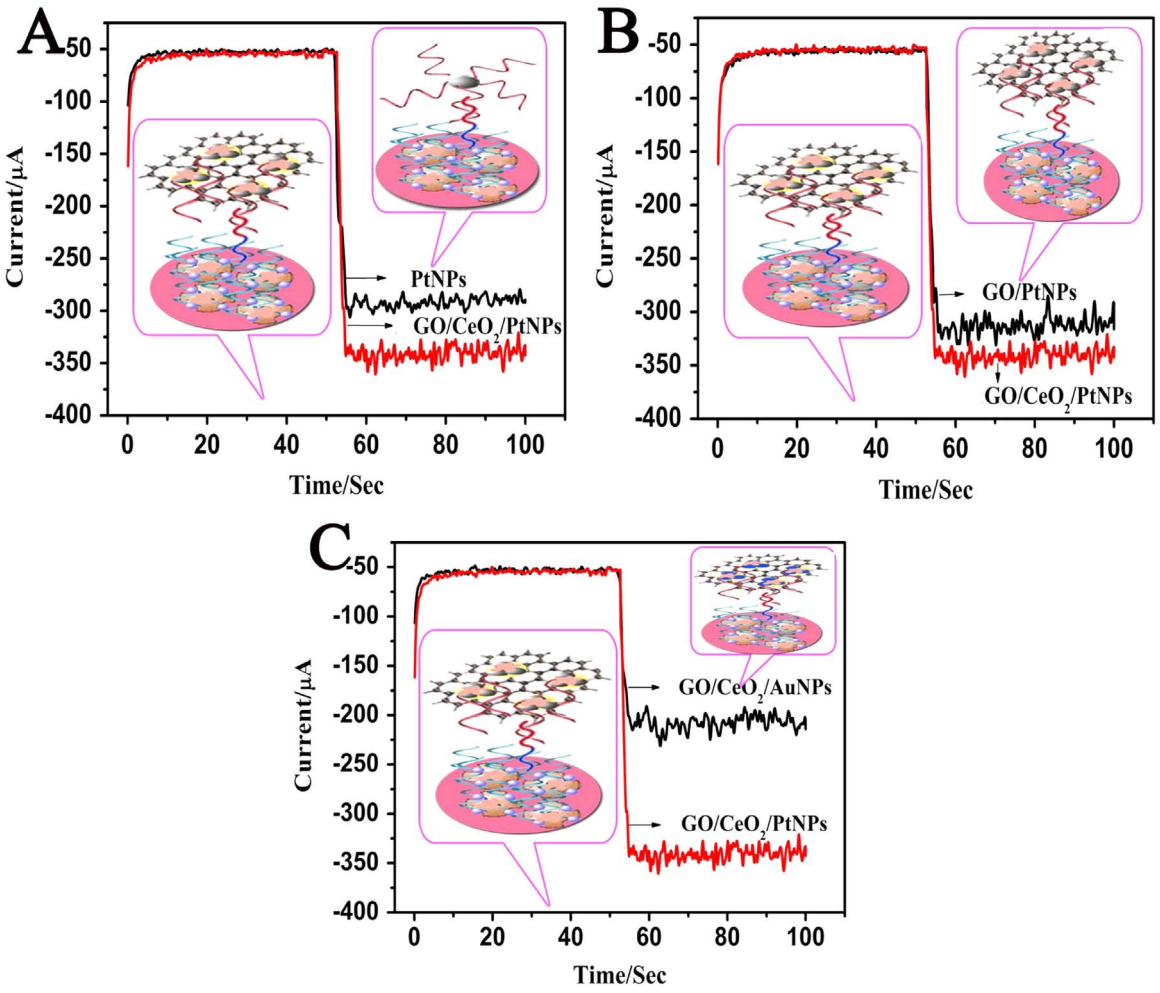

Fig. 4. Amperometric i-t curves of different nanomaterials after the format bioreaction of the proposed biosensor in the presence of 100 fM target DNA: (A) catalysis of PtNPs/SP and GO/CeO_2/PtNPs/SP; (B) catalysis of GO/PtNPs/SP and GO/CeO_2/PtNPs/SP; (C) catalysis of GO/CeO_2/AuNPs/SP and GO/CeO_2/PtNPs/SP. They were all detected in 7 mL of PBS (PH 7.4) with the addition of H_2O_2 (1.4 mol L^{-1}).

types of SP-functionalized detect probes (1) PtNPs/SP, (2) GO/PtNPs/SP, and (3) GO/CeO_2/AuNPs/SP were prepared to compare with the proposed detect probe. The same batch of biosensors were incubated with the 100 fM target DNA and were then incubated with differently labelled signal tag solutions. As shown in Fig. 4A, the current response of the biosensor with GO/CeO_2/PtNPs/SP was improved in comparison with that of the biosensor with PtNPs/SP. This improvement may be ascribed to the catalytic activity of CeO_2 and PtNPs toward H_2O_2. Moreover, when the biosensor was incubated with GO/PtNPs/SP in Fig.4 B, the current response was enhanced compared with that of PtNPs/SP. Due to the fact that GO have large surface areas, which makes them good at carrying nanoparticles (Xu et al., 2015). When compared with GO/CeO_2/PtNPs/SP, the current response of GO/PtNPs/SP was smaller. This result is ascribed to the catalytic activity of CeO_2 toward H_2O_2 and also indicated the fact that the GO/CeO_2/PtNPs hybrid nanomaterial enhanced the catalytic ability toward H_2O_2 (Zhang et al., 2012). More interestingly, compared with GO/CeO_2/AuNPs/SP in Fig.4C, the current response was remarkably increased when the biosensor was successively incubated with GO/CeO_2/PtNPs/SP. The reason for this was that catalysis of CeO_2 and PtNPs greatly enhanced the current response and demonstrated promising characteristics in the signal amplification system. Therefore, we chose GO/CeO_2/PtNPs/SP as the signal tag throughout the experiment.

3.6. Optimization of the experimental conditions

To ensure the high performance of the biosensor, several parameters involved in the experiments, such as the concentration of SA, immobilization time of CP, incubation time and the concentration of H_2O_2 were investigated.

The concentration of SA is a rather important factor for biosensor fabrication and could influence its stability and sensitivity. As shown in Fig. S3A, the current response decreased rapidly with increasing SA concentrations from 40 μg mL^{-1} to 100 μg mL^{-1}. A further increase of the concentration of SA had no significant effect on the current change which indicating that the maximum immobilization of SA was obtained. In this experiment, the electrodeposition was performed in a 1.0 wt% $HAuCl_4$ solution at −0.2 V for 30 s. Therefore, 100 μg mL^{-1} was chosen as the optimal concentration of SA.

In addition, to achieve an optimal electrochemical signal, the immobilization time of CP was tested. Hence, the immobilization time of CP was investigated in Fig. S3B. With the increase of immobilization time, the current responses for the biosensor first increased quickly and then remained steady at approximately 12 h, indicating that the maximum immobilization of CP was obtained. In this experiment, the electrodeposition was performed in a 1.0 wt% $HAuCl_4$ solution at −0.2 V for 30 s and the concentration of SA was 100 μg mL^{-1}. To completely hybridize the target DNA in the following step, 12 h was chosen as the optimal immobilization time.

For target DNA recognition, the incubation time is an extremely important parameter. With an increase in incubation time, the current responses first increased and were saturated when the incubation time reached 2 h (Fig. S3C). The lower responses were attributed to the lack of maximum formation of sandwich complexes. In this experiment, the electrodeposition was performed in a 1.0 wt% $HAuCl_4$ solution at −0.2 V for 30 s, the concentration of SA was 100 μg mL^{-1} and the immobilization time of CP was 12 h. Therefore, 2 h was chosen as the optimal incubation time.

Furthermore, the concentration of H_2O_2 was optimized by recording the i-t responses when adding different concentrations of H_2O_2 (from 0.8 to 1.8 mol L^{-1}) to the electrolyte with PBS (7 mL, pH 7.4). Fig. S3D shows that the peak current increased with the increase in H_2O_2 and then tended to reach saturation after adding 1.4 mol L^{-1} of H_2O_2, predicating the highest efficiency of bioelectrocatalysis at this point. In this experiment, the electrodeposition was performed in a 1.0 wt% $HAuCl_4$ solution at −0.2 V for 30 s, the concentration of SA was 100 μg mL^{-1}, the immobilization time of CP was 12 h and the incubation time was 2 h. Thus, 1.4 mol L^{-1} of H_2O_2 was employed throughout the detection process.

3.7. Analytical performance of the DNA biosensor

Under the optimized experimental conditions, the analytical performance of the proposed biosensor with different concentrations of target DNA is shown in Fig. 5. The electrochemical signal gradually increased with increasing concentrations of target DNA in 7 mL of PBS (0.1 M, pH 7.4) containing 1.4 mol L^{-1} of H_2O_2, as shown in Fig. 5A and B. As shown in Fig. 5A, the current changes increased with the increment of target DNA (ADRB1−1165 G > C) from 1 fM to 100 fM, and the same trend is shown in Fig. 5B from 100 fM to 10 nM. As shown in Fig. 5C, the calibration plot was divided into two linear sections. The linear regression equation was Y=188.19+43.77*X in the range from 1 fM to 100 fM and Y=220.59+28.27*X in the range from 100 fM to 10 nM in the detection of ADRB1. The detection limits were estimated to be 0.33 fM at a signal-to-noise ratio of 3σ (where σ is the standard deviation of the blank, n=10), which is slightly lower than those of other reported studies. The lower detection limits might be attributed to the catalytic performance of CeO_2, PtNPs and the biotin-avidin system, which greatly amplified the peak signals. A comparison of the proposed biosensors with other methods in the literature is shown in Table S3, and the proposed method enabled a faster detection efficiency of ADRB1. To better show the advantages of this DNA sensor, the associated performance parameters (e.g., responsive strategy, detection limit, linear range) have been compared with those obtained by other similar strategies and listed in Table S4. To further confirm the effect of the biotin-avidin system, another calibration plot was constructed using AuNPs/CP as the platform. As shown in Fig. 5D, the currents decreased with increased concentrations in the range from 100 fM to 1 nM, and the calibration plots between the current change and the logarithm of target DNA displayed good linear relationships with the regression equation: Y=234.40+12.59*X, R^2=0.9995 in Fig.5 E. Additionally, the detection limit of ADRB1 was 33 fM, which was higher than that of the biosensor that we used in this research. This result may be attributed to SA providing more sites for conjunction with bio-CP, thus improving the current response. A comparison of the analytical figure of merit for the different types of sensors clearly demonstrated that the presence of SA enabled a bio-sensing performance that was superior to that observed in the absence of SA.

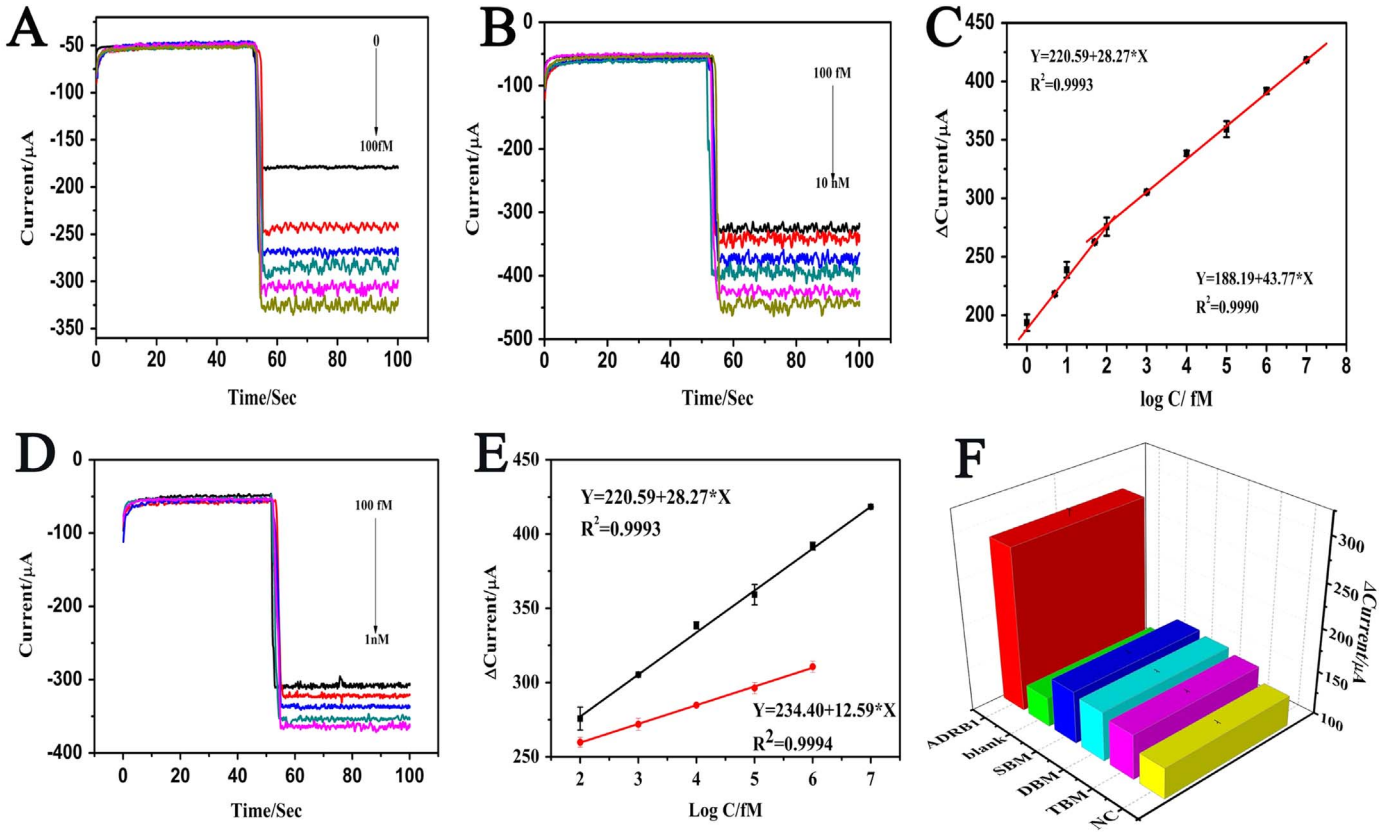

Fig. 5. The Amperometric i-t curves of the proposed biosensor with different target DNA concentrations in 7 mL of PBS (pH 7.4) with the addition of H_2O_2 (1.4 mol L^{-1}): (A) 0–100 fM, (B)100 fM–10 nM; (C) calibration curve of the biosensor toward different concentrations of target DNA; (D) the amperometric i-t curves of the biosensor without SA and incubated with different target DNA concentrations from 100 fM–1 nM in 7 mL of PBS (pH 7.4) with the addition of H_2O_2 (1.4 mol L^{-1}); (E) a comparison of the calibration curves obtained for the two types of strategies for target DNA. (F) The specificity of the biosensor was investigated with four types of 10 nM ssDNA: single-base mismatched DNA (SBM), double-base mismatched DNA (DBM), three-base mismatched DNA (TBM), non-complementary DNA (ncDNA) and blank control. Error bars are the standard deviations across three repetitive experiments.

3.8. Specificity, stability and reproducibility of the DNA biosensor

The specificity of the proposed biosensor was evaluated by incubation with target DNA, single-base mismatch (SBM, wild type), double-base mismatch (DBM), three-base mismatch (TBM), non-complementary target (random) and blank controls. As summarized in Fig. 5F, with an excess (10-fold) amount of nontarget analytes, the proposed biosensor exhibited negligible interference to the above mismatched targets. The results indicated the high affinity of the biosensor to its complementary DNA target and that the developed biosensor could discriminate different DNA sequences effectively through the principle of complementary base pairing.

Long-term storage stability was assessed at 3-day, 7-day, 14-day, 21-day and 28-day periods while the electrochemical biosensor was stored as shown in Fig. S4A. The peak current retained 99.3%, 97.9%, 96.8%, 95.7%, and 94.7% of the original value, respectively. These results indicated that the stability of the assay system was acceptable.

The reproducibility of the biosensor was investigated by relative standard derivations (RSD) of inter- and intra-analysis using 100 fM target DNA (Fig. S4B). The results were estimated using one biosensor for five assays and three biosensors for one assay. The inter-assay RSD value was 1.28%, and the intra-assay RSD value was 1.53%. These results indicate that the proposed bioassay possesses acceptable precision and reproducibility.

3.9. Preliminary application of the DNA biosensor

The ultimate goal of developing a mutation-discriminating biosensor was to enable the direct analysis of mutated sequences in patient samples. Therefore, the biosensor was used to test the recovery of three concentrations of ADRB1 in human serum samples, referencing the reported methods (Liu et al., 2015). Three concentrations (1 fM, 1 pM and 1 nM) of ADRB1-spiked human serum samples were prepared. The plasma samples were diluted to suitable concentrations with pH 7.4 PBS (1:10). It can be seen in Table S5 that the relative standard deviations were in the range of 2.06–2.3% and that the recoveries were in the range of 99.4–101.9%. These results show that the developed biosensor might be preliminarily applied to determine the presence of ADRB1 in real samples.

4. Conclusion

In summary, an ultrasensitive DNA biosensor was successfully developed for the bioassay of ADRB1 using GO/CeO_2/PtNPs as a signal probe. The developed biosensor has a broad linear range with a low detection limit and high specificity, suggesting resilience against endogenous interference in human serum. At the same time, it demonstrates high sensitivity and good reproducibility, making it a potentially advantageous tool for clinical research. Furthermore, the biosensor will promote the greater use of CeO_2 nanoparticles in the biosensing field. However, the biosensor requires multiple modification steps, which may limit its use. Therefore, it is necessary to reduce some of the steps to enhance its application in the biosensing field, which requires finding a breakthrough to simplify the modification steps, such as co-deposition and the antedating response.

Acknowledgements

We are grateful for the financial support from the National Nature Science Foundation of China (No. 81370403), Chongqing foundation and advanced research project (No. CSTC2015jcyjBX0053), and Chongqing medical university scientific research cultivating fund(No. 201414).

Appendix A. Supplementary material

Supplementary data associated with this article can be found in the online version at http://dx.doi.org/10.1016/j.bios.2016.10.087.

References

Carson, S., Wanunu, M., 2015. Nanotechnology 26, 074004.
Dong, X.Y., Mi, X.N., Zhang, L., Liang, T.M., Xu, J.J., Chen, H.Y., 2012. Biosens. Bioelectron. 38, 337–341.
Gao, L., He, J., Xu, W., Zhang, J., Hui, J., Guo, Y., Li, W., Yu, C., 2014. Biosens. Bioelectron. 62, 79–83.
Jiang, Q., Yuan, H., Xing, X., Liu, J., Huang, Z., Du, X., 2011. Indian J. Biochem. Biophys. 48, 301–307.
Kang, S., Hong, X., Ruan, C.W., Yu, P., Yu, S.S., Chen, M., Zhang, D.F., Fan, H.M., Liu, Z.M., 2015. J. Transl. Med. 13, 44.
Li, Y., Deng, J., Fang, L., Yu, K., Huang, H., Jiang, L., Liang, W., Zheng, J., 2015. Biosens. Bioelectron. 63, 1–6.
Li, Q., Yu, C., Gao, R., Xia, C., Yuan, G., Li, Y., Zhao, Y., Chen, Q., He, J., 2016. Biosens. Bioelectron. 80, 674–681.
Lima, J.J., Feng, H., Duckworth, L., Wang, J., Sylvester, J.E., Kissoon, N., Garg, H., 2007. Metabolism 56, 757–765.
Liu, L., Song, C., Zhang, Z., Yang, J., Zhou, L., Zhang, X., Xie, G., 2015. Biosens. Bioelectron. 70, 351–357.
Nicoulina, S., Shulman, V., Shesternya, P., Chernova, A., Salmina, A., Issachenko, O., Maksimov, V., Voevoda, M., 2010. Genet. Test. Mol. Biomark. 14, 249–253.
Tang, J., Chen, X., Zhou, J., Li, Q., Chen, G., Tang, D., 2013. Analyst 138, 4327–4333.
Thomas, K.L., Ellingrod, V.L., Bishop, J.R., Keiser, M.J., 2010. Psychopharmacol. Bull. 43, 11–22.
Ujjain, S.K., Das, A., Srivastava, G., Ahuja, P., Roy, M., Arya, A., Bhargava, K., Sethy, N., Singh, S.K., Sharma, R.K., Das, M., 2014. Biointerphases 9, 031011.
Wei, Y., Li, Y., Li, N., Zhang, Y., Yan, T., Ma, H., Wei, Q., 2016. Biosens. Bioelectron. 79, 482–487.
Xu, W., He, J., Gao, L., Zhang, J., Hui, J., Guo, Y., Li, W., Yu, C., 2015. J. Electroanal. Chem. 741, 8–13.
Yang, Z., Zhu, J., Dai, H., Li, J., Shen, J., Jiao, X., Hu, X., Ju, H., 2014. Biosens. Bioelectron. 51, 356–361.
Zhang, Y., Hou, F., Tan, Y., 2012. Chem. Commun. 48, 2391–2393.
Zhang, J., Yuan, Y., biXie, S., Chai, Y., Yuan, R., 2014. Biosens. Bioelectron. 60, 224–230.
Zhu, Q., Chai, Y., Zhuo, Y., Yuan, R., 2015. Biosens. Bioelectron. 68, 42–48.